

## Temperature dependence of surface layering in a dielectric liquid

Haiding Mo,<sup>1</sup> Sumit Kewalramani,<sup>2</sup> Guennadi Evmenenko,<sup>2</sup> Kyungil Kim,<sup>2</sup> Steven N. Ehrlich,<sup>1</sup> and Pulak Dutta<sup>2</sup>

<sup>1</sup>*National Synchrotron Light Source, Brookhaven National Laboratory, Upton, New York 11973, USA*

<sup>2</sup>*Department of Physics and Astronomy, Northwestern University, Evanston, Illinois 60208, USA*

(Received 23 October 2006; revised manuscript received 16 February 2007; published 24 July 2007)

The temperature dependence of the density oscillations (layers) at the free surface of tetrakis(2-ethylhexoxy)silane, a nonmetallic molecular liquid, was investigated using x-ray reflectivity. Below  $\sim 215$  K, the layer parameters weakly vary with temperature, if at all. Above this temperature, the layer spacings and intrinsic layer widths increase continuously, until there is no identifiable layering above 230 K. This transition occurs at  $T/T_c \approx 0.23$ , a temperature region that is usually accessible in metallic liquids but is preempted by freezing in many dielectric liquids.

DOI: [10.1103/PhysRevB.76.024206](https://doi.org/10.1103/PhysRevB.76.024206)

PACS number(s): 68.03.Hj, 68.15.+e

### I. INTRODUCTION

It has been established both theoretically<sup>1-3</sup> and experimentally<sup>4-7</sup> that the surfaces of metallic liquids are layered. On the other hand, many studies of normal dielectric liquid free surfaces near room temperature showed no evidence of layering. The work of Rice *et al.*<sup>1-3</sup> predicted this difference and attributed it to the presence of an electron gas in liquid metals. Recently, however, Chacón and co-workers<sup>8-10</sup> concluded from Monte Carlo simulations that surface layering is a universal property of liquids: the surface layering can be observed if the temperature is below  $\sim 0.2T_c$ , where  $T_c$  is the critical temperature. This effect has also been seen in simulations by Li and Rice.<sup>11</sup> This temperature is usually easily accessible in liquid metals because  $T_c$  is high, but in many dielectric liquids it lies well below the freezing point.

The prediction of Chacón and co-workers has been confirmed by our recent x-ray reflectivity study of tetrakis(2-ethylhexoxy)silane (TEHOS), an isotropic nonconducting molecular liquid that does not freeze until very low temperatures.<sup>12</sup> We saw that at higher temperatures the density of TEHOS surface changes monotonically normal to the surface, just as in other dielectric liquid surfaces.<sup>13-18</sup> However, at lower temperatures, reflectivity oscillations appear, indicating that layers have formed. The layering extends only 4–5 molecular diameters into the bulk, similar to the layering at metallic surfaces, and distinct from liquid crystal surfaces where the surface layering can extend hundreds of angstroms into the bulk.<sup>19,20</sup>

A number of mechanisms have been proposed to explain liquid surface layering. For example, after comparing the pair correlation function in different liquids, Soler *et al.*<sup>21</sup> proposed that pronounced density oscillations appear if the liquid-vapor interface is sharp. In our study of the TEHOS surface, we found that there is a surface region with average density higher than the bulk density when layering appears, which is different from the layering in many metallic liquids<sup>12</sup> although somewhat similar to that reported in liquid Sn.<sup>7</sup> It is conceivable that layering in dielectric liquids and layering in metallic liquids have entirely different origins. Analysis of the temperature dependence of the layer structure at metallic surfaces has shown that it is possible to determine

whether there are temperature-dependent components in addition to the inevitable capillary wave broadening that reduces the amplitude of the observed layering peak.<sup>22,23</sup> Therefore, a study of the temperature dependence of surface layering in a dielectric liquid should be helpful as input to future theoretical work on the origins of surface layering.

We now have done a much finer-grained study as a function of temperature than in our earlier paper.<sup>12</sup> Moreover, we were able to obtain a better estimate of the capillary broadening, so we have now plotted the intrinsic layering parameters with capillary broadening deconvoluted. This has made visible trends that could not be discerned in the data shown in Ref. 12.

### II. EXPERIMENTAL DETAILS

TEHOS was purchased from GLEST Inc. with a purity of  $>95\%$  and used as supplied. The molecule has a diameter of about  $10 \text{ \AA}$ . Its freezing temperature and its critical temperature have not been precisely determined, but viscosity measurements<sup>24</sup> indicate that it is a fluid down to at least 219 K. As previously reported,<sup>12</sup> we saw no evidence of a bulk phase transition down to 190 K in either transmission x-ray data or differential scanning calorimetry data. The critical point  $T_c$  is estimated to be  $\sim 950 \text{ K}$ .<sup>12,25</sup>

In order to do this experiment in a closed-cycle refrigerator, we prepared  $\sim 5000 \text{ \AA}$  films of TEHOS supported on silicon substrates.<sup>26</sup> This is for all practical purposes a bulk liquid since the film thickness is much larger than the substrate roughness, molecular dimensions, etc. TEHOS has an extremely low evaporation rate, and we saw no measurable thickness change over  $\sim 12 \text{ h}$ .

It is known that TEHOS forms layers near smooth silicon surfaces.<sup>26,27</sup> To eliminate features in the reflectivity due to this interface layering, we prepared and used substrates with rms surface roughness  $>20 \text{ \AA}$ . This causes the scattering features due to interfacial layers to contribute only a diffuse background to the reflectivity data.<sup>26</sup> We have confirmed that the specular reflectivity signal from the rough silicon surface rapidly drops with  $Q$  and is negligible at  $Q > 0.15 \text{ \AA}^{-1}$  compared to the scattering from the free liquid surface. The method of preparation of the rough silicon wafers has been described previously.<sup>12</sup>

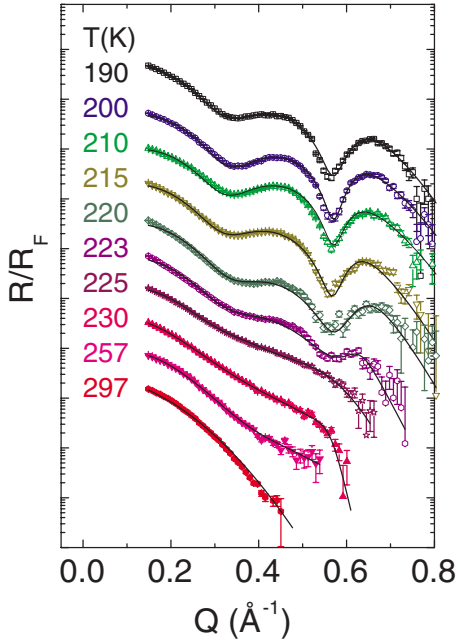


FIG. 1. (Color online) The specular reflectivity (normalized to the Fresnel reflectivity) at various temperatures. The solid curves are the best fits to the data using the model described in the text [Eq. (1)] except for the data at 297 K, which are fitted to an error-function-type electron density profile since there is no evidence of layering. The curves are displaced vertically for clarity.

Specular x-ray reflectivity studies were performed at MATRIX (beamline X18A, National Synchrotron Light Source). The beam size was  $\sim 0.8$  mm vertically and  $\sim 1$  mm horizontally. The momentum resolution was  $\sim 0.006$   $\text{\AA}^{-1}$ . More details regarding sample mounting and data collection are in Ref. 12.

### III. RESULTS

Figure 1 shows the specular reflectivity  $R$  normalized to the Fresnel reflectivity  $R_F$ , at ten different temperatures from 190 to 297 K. At 230 K and below, one sees some structure in the reflectivity curves. The specular peak near  $0.63$   $\text{\AA}^{-1}$  is at the same  $Q$  as the TEHOS bulk (isotropic) peak. One sees from Fig. 1 that there is not much change in the specular reflectivity curves below 215 K. Above this temperature, the height of layering peak drops significantly. At 230 K, only a very weak hump is visible, and at higher temperatures the curves become featureless. (Surface roughness prevents us from collecting significant data at higher  $Q$  at these temperatures.) This temperature region corresponds to  $T/T_c \sim 0.23$ . While the main features of the reflectivity curves match well with the results reported previously,<sup>12</sup> the temperature above which surface layering vanishes is several degrees lower in the data we now report. The reason for this small discrepancy is unknown, but the data shown here are reproducible (see below).

Figure 2 shows the peaks in specular reflectivity data and bulk scattering data. In specular reflectivity data, the bulk scattering background has been subtracted. Comparing the

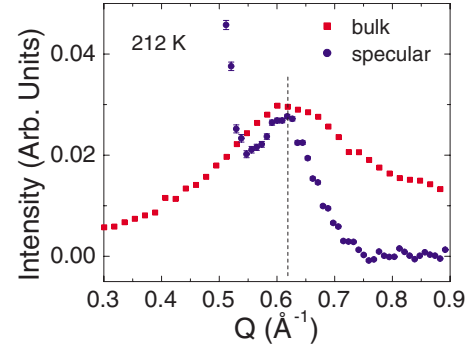


FIG. 2. (Color online) Comparison of the peak in the specular reflectivity with that in the bulk data (taken in transmission geometry). Both data were collected at 212 K. In the case of the specular reflectivity, the off-specular background has been subtracted.

layering peak in the specular reflectivity curve to the bulk liquid scattering peak near  $0.63$   $\text{\AA}^{-1}$ , one sees clearly that the width of the specular peak is much smaller ( $\sim 0.1$   $\text{\AA}^{-1}$ ) than that of the bulk peak ( $\sim 0.25$   $\text{\AA}^{-1}$ ), indicating that there is longer-range order along the surface normal direction compared to the order in the bulk liquid.

We fitted the data following a modified version of the distorted-crystal model. The original model<sup>4,5,22</sup> has been used to fit data from a number of liquid metal surfaces and offers a way to deconvolute capillary interface broadening. We use the modified function:<sup>12</sup>

$$\frac{\rho}{\rho_{\text{bulk}}} = r \sum_{n=0}^1 \frac{d_0}{\sqrt{2\pi}\sigma_n} e^{-(z+nd_0)^2/2\sigma_n^2} + \sum_{n=2}^{\infty} \frac{d_1}{\sqrt{2\pi}\sigma_n} e^{-[z+(n-2)d_1+2d_0]^2/2\sigma_n^2}, \quad (1)$$

where  $\sigma_n^2 = \sigma_0^2 + n\bar{\sigma}^2$ , and  $\sigma_0$  is the width of the first layer, which combines two terms:  $\sigma_0^2 = \sigma_i^2 + \sigma_{\text{cw}}^2$ , where  $\sigma_{\text{cw}}$  is due to thermal capillary waves and  $\sigma_i$  is an intrinsic term due to all other factors. Compared to the original model,<sup>4,5,22</sup> we have introduced two additional parameters. The first one is the spacing between the first three layers ( $d_0$ ), which is allowed to be different from that between layers further inside the bulk liquid ( $d_1$ ); the second parameter ( $r$ ) is used to account for the different electron density in the first two layers.

Note that  $\sigma_{\text{cw}}$  is not a variable parameter in our fits. We have measured the surface tension near and below room temperature using the Wilhelmy-plate method in the range 265–305 K (Fig. 3, top panel). We then extrapolated it to the temperatures of interest<sup>28</sup> using the Pitzer-type function  $\ln \gamma = A + n \ln(T_c - T)$  and used this to calculate the capillary contribution to the interface width<sup>29</sup> as a function of temperature. The calculated  $\sigma_{\text{cw}}$  is shown in Fig. 3 (bottom panel).

Excellent fits, shown as solid curves in Fig. 1, are obtained with this model. The unmodified model<sup>4,5,22</sup> would fail to fit the extra peak at  $\sim 0.44$   $\text{\AA}^{-1}$  in our data. The actual fitted electron densities are not shown here, but typical fits are in Fig. 2 of Ref. 18. At lower temperatures (215 K and

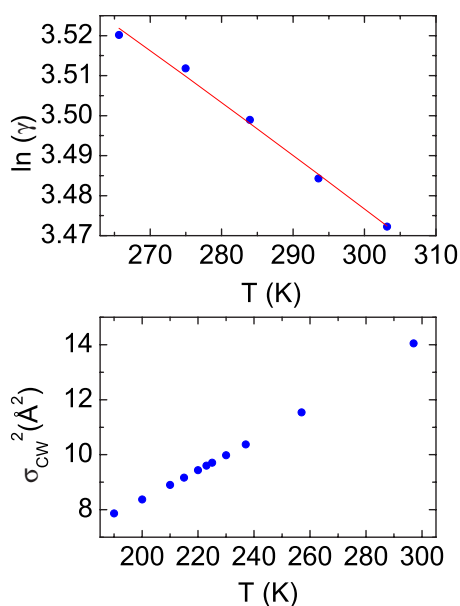


FIG. 3. (Color online) (a) TEHOS surface tension  $\gamma$  measured at and below room temperature. Fitting model:  $\ln(\gamma) = A + n \ln(T_c - T)$ , where  $T_c$  is fixed at 950 K. The best fit gives  $A = -2.20$  and  $n = 0.88$ . (b) The calculated square of capillary wave roughness  $\sigma_{CW}^2$ , with  $q_{max} = 0.4 \text{ \AA}^{-1}$ , at the low-temperature range of interest. The roughness was derived from the surface tension obtained by extrapolating the fitting function in (a) to low temperatures.

below), there is a higher-density layer of about  $20 \text{ \AA}$  thickness at the surface (average density in this layer is about 15% higher than that in the bulk) and several distinct oscillations in the electron density profile. Above 215 K, the density oscillation amplitude starts to drop, and 230 K is the highest temperature at which any oscillations can be seen. As the amplitude of the oscillations decreases, the density in the surface layer also drops significantly. At 230 K, the mean density of the surface region has dropped to that of the bulk liquid.

Compared to the surface layering observed in liquid metals, the density oscillation amplitudes (see, e.g., Fig. 2 of Ref. 18) are smaller fractions of the bulk density. This may be due to the extended nature of the molecule, which “smears” the electron density. The temperature dependence of layering on the TEHOS surface is somewhat similar to that observed for liquid metals previously.<sup>22,23</sup> In both cases, the surface layering continuously weakens as temperature increases. However, in TEHOS, the layering drops much more rapidly above a threshold temperature, and this may be consistent with a continuous transition. The region nearest the surface is denser on average than the bulk liquid. Theoretical work has suggested that the surface atoms have a tendency to move closer to each other, and this higher lateral packing induces a density oscillation which propagates several atomic diameters into the bulk.<sup>30,31</sup> The increased average density at the TEHOS surface may be a manifestation of such a mechanism (see Ref. 7).

While the distorted-crystal model elegantly allows us to deconvolute the effect of capillary surface broadening and see what the intrinsic density oscillations would look like, it

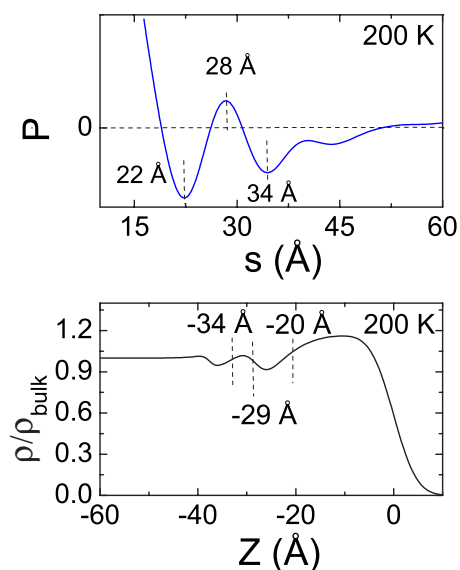


FIG. 4. (Color online) Patterson function (top) and the electron density profile obtained from the slab model fit (bottom) for data at 200 K. The vertical dashed lines in the top and bottom figures indicate the maxima and minima in the Patterson function and correspond to internal “interfaces” in the liquid.

is important to establish that the basic conclusions are independent of the model used. We show in Fig. 4 the Patterson function<sup>32</sup> of the  $R(q)/R_F(q)$  data at 200 K:

$$P(s) = \frac{1}{2\pi} \int_{-\infty}^{\infty} dq \frac{R(q)}{R_F(q)} e^{-iqs} = \frac{1}{\rho_0^2} \int_{-\infty}^{\infty} \left\langle \frac{d\rho(z)}{dz} \right\rangle \times \left\langle \frac{d\rho(s+z)}{dz} \right\rangle dz. \quad (2)$$

A maximum or minimum in the Patterson function at a given  $s$  indicates that there are two interfaces a distance  $s$  apart; if the density is changing in the same direction at both interfaces, one sees a maximum, while if one is increasing while the other is decreasing, one sees a minimum. It can be seen in Fig. 4 that there are two distinct minima and one distinct maximum. Since the free surface has the largest density change, these strong turning points indicate the positions of internal “interfaces” as measured from the liquid-air interface. There is one internal interface where the electron density change is in the same direction as at the free surface, and two internal interfaces where the electron density change is in the opposite direction. The first minimum in the Patterson function is unusually deep, which indicates that there is a denser layer at the surface when the layering occurs. The Patterson functions for data at other temperatures below the layering transition share similar features.

These features are clearly reproduced in a traditional “slab model” fit (Fig. 4, lower panel) using three surface slabs of different electron densities, thicknesses, and interface widths in addition to the semi-infinite bulk liquid. There are interfaces at distances of 20, 29, and  $34 \text{ \AA}$  below the liquid-vapor interface. We have also performed a “model-independent” fit<sup>33</sup> using  $18 \times 4 \text{ \AA}$  slabs whose densities vary independently.

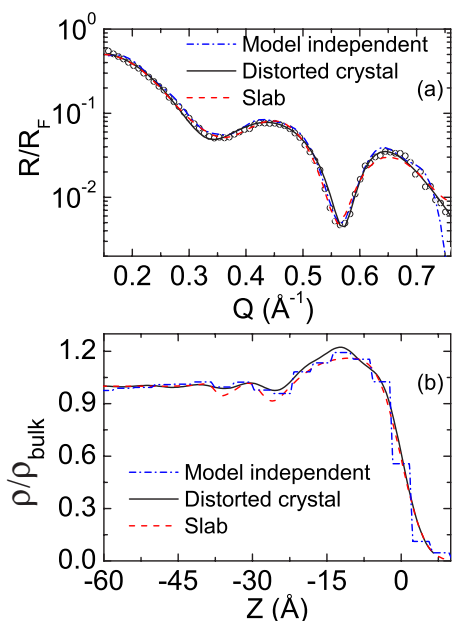


FIG. 5. (Color online) Comparison of the results obtained using different fitting methods, for the data at 200 K: (a) the specular reflectivity and (b) the calculated electron density.

Figure 5 shows the best fits with each method (top panel) and the electron density profiles from each method (bottom panel). (The distorted-crystal-model density is shown without removing the capillary broadening.) It can be seen that all fitting methods show the same basic features. There are density oscillations indicating layering, and there is a density increase in the first  $\sim 20$  Å below the surface, corresponding roughly to one bilayer of TEHOS molecules.

We now return to our modified distorted-crystal fit [Eq. (1)] and show the temperature dependence of the relevant fitting parameters (Fig. 6). Data from two different runs are shown using different symbols to indicate the degree of re-

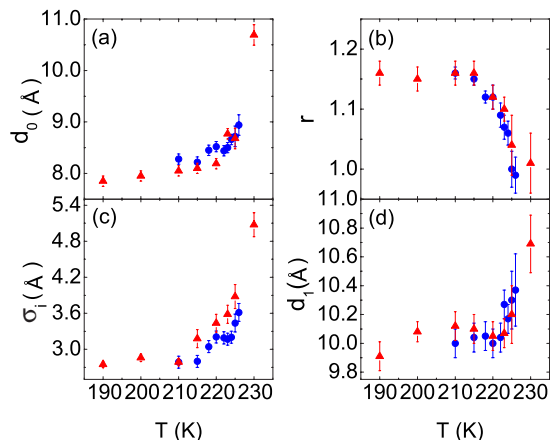


FIG. 6. (Color online) Temperature dependence of the fitting parameters.  $d_0$  and  $d_1$  are the spacings between the first three layers and between subsequent layers, respectively;  $r$  is the relative density of the surface layer; and  $\sigma_i$  is the intrinsic roughness in the first layer. [See Eq. (1) and associated discussion.] The two different symbols refer to results from two different runs.

producibility. In both runs, the data were collected by first cooling the sample to the lowest temperature, and then raising the sample temperature to the desired point where it is then held constant. It should be noted that at a liquid surface, the observed roughness depends on the experimental resolution.<sup>34</sup> The present experiments were performed with a  $q_z$  resolution of  $0.006 \text{ \AA}^{-1}$ .

One sees in Fig. 6(a) that  $d_0$  is about  $8.0 \text{ \AA}$  at 215 K and below, and hardly changes in the low-temperature region. The spacing  $d_0$  is  $\sim 2 \text{ \AA}$  less than the spacing  $d_1$  [Fig. 6(d)]. Both  $d_0$  and  $d_1$  increase as the temperature rises above 215 K. Similarly,  $\sigma_i$  sharply increases above 215 K [Fig. 6(c)], while the surface density enhancement [Fig. 6(b)] decreases. The fact that  $\sigma_i$  rapidly increases as the layering disappears suggests that it may be the increase in layer width that smears the features and thus weakens the density variations. The intrinsic width  $\sigma_i$  and the capillary wave vector cutoff  $q_{\text{max}}$  are usually coupled.<sup>8</sup> When  $\sigma_i$  rapidly increases (i.e., above 223 K),  $q_{\text{max}}$  should change in this temperature range, and using a constant  $q_{\text{max}}$  to calculate  $\sigma_{\text{cw}}$  may not be appropriate. However, the fact that  $\sigma_i$  is nearly constant below 215 K and rapidly increases above it (even assuming fixed  $q_{\text{max}}$ ) clearly shows that factors other than capillary wave broadening are playing a role. The parameter  $\bar{\sigma}$  has not been plotted: below 215 K, it was constant at  $1.9 \pm 0.1 \text{ \AA}$ , but above this temperature the uncertainty becomes very large because the layering features are so weak. The higher-temperature fits shown were done with  $\bar{\sigma}$  fixed at the lower-temperature value. It can be seen in Fig. 6(d) that the uncertainty in the layer spacing  $d_1$  is also very large at higher temperatures.

As pointed out in Ref. 12, the coupling between the monotonic increase of  $\sigma_i$  with temperature and the loss of layering suggests that the layering is not caused by the impurity segregation at the surface. Impurities would decrease the surface energy (surface tension), which would cause an increase in the apparent intrinsic surface width. This is the opposite of what we observe.

We have previously performed in-plane scattering to look for lateral order at the surface.<sup>12</sup> No peaks other than the liquidlike bulk peaks were observed, and the horizontal width of the liquid like peaks is comparable to that of the peaks in bulk scattering, which indicates that there is no enhanced lateral order at the surface. This is similar to the surface layering in liquid metals and distinct from surface freezing, a pretransition effect in which quasi-long-range lateral order is seen.<sup>35</sup>

The temperature region at which we observed layering in TEHOS corresponds to a reduced temperature  $T/T_c \sim 0.23$ , which is close to the threshold  $T/T_c \sim 0.15-0.2$  seen in the simulations of Chacón and co-workers.<sup>8-10</sup> The small discrepancy could be due to the difference in size of TEHOS ( $\sim 10 \text{ \AA}$ ) and the molecule used in the simulation ( $\sim 3.3 \text{ \AA}$ ). It has been shown in one simulation that the amplitude of layer oscillations increases with the size of the molecule.<sup>10</sup> We also note that the simulations do not show a denser layer at the surface as observed for TEHOS, and this may be related to the shift in threshold temperature. In other words, the actual TEHOS surface may be somewhat more complicated than the theoretical model. However, our results are in quali-

tative agreement with the simulations in that layering appears at low  $T/T_c$  even in nonmetallic liquids if the liquid does not freeze. The simulations do not have the temperature resolution of the experiments reported here, and therefore there are no specific theoretical predictions regarding the trends shown in Fig. 6.

#### IV. CONCLUSIONS

Surface layering in a dielectric liquid, TEHOS, occurs below  $\sim 230$  K. When layering occurs, a denser layer appears at the surface, with a 20% smaller layer spacing in this denser layer. The amplitude of the density oscillations drops continuously but rapidly as the temperature increases. Fitting

results show that the spacing of the layers nearest to the surface rapidly increases with temperature in the transition region. Simultaneously, the roughness of the first layer dramatically increases, much faster than the increase attributable to capillary waves alone.

#### ACKNOWLEDGMENTS

This work was supported by the U.S. National Science Foundation under Grant No. DMR-0705137. Use of the National Synchrotron Light Source (NSLS) is supported by the U.S. Department of Energy under Contract No. DE-AC02-98CH10886. The MATRIX beamline at NSLS is also supported by the U.S. Department of Energy.

- 
- <sup>1</sup>S. A. Rice, D. Guidotti, H. L. Lemberg, W. C. Murphy, and A. N. Bloch, in *Advances in Chemical Physics XXVII*, edited by I. R. Prigogine and S. A. Rice (Wiley, New York, 1974).
- <sup>2</sup>M. P. D'Evelyn and S. A. Rice, *Phys. Rev. Lett.* **47**, 1844 (1981).
- <sup>3</sup>S. A. Rice, *Mol. Simul.* **29**, 593 (2003).
- <sup>4</sup>O. M. Magnussen, B. M. Ocko, M. J. Regan, K. Penanen, P. S. Pershan, and M. Deutsch, *Phys. Rev. Lett.* **74**, 4444 (1995).
- <sup>5</sup>M. J. Regan, E. H. Kawamoto, S. Lee, P. S. Pershan, N. Maskil, M. Deutsch, O. M. Magnussen, B. M. Ocko, and L. E. Berman, *Phys. Rev. Lett.* **75**, 2498 (1995).
- <sup>6</sup>H. Tostmann, E. DiMasi, P. S. Pershan, B. M. Ocko, O. G. Shpyrko, and M. Deutsch, *Phys. Rev. B* **59**, 783 (1999).
- <sup>7</sup>O. G. Shpyrko, A. Y. Grigoriev, C. Steimer, P. S. Pershan, B. Lin, M. Meron, T. Graber, J. Gerbhardt, B. Ocko, and M. Deutsch, *Phys. Rev. B* **70**, 224206 (2004).
- <sup>8</sup>E. Chacón, M. Reinaldo-Falagán, E. Velasco, and P. Tarazona, *Phys. Rev. Lett.* **87**, 166101 (2001).
- <sup>9</sup>R. Checa, E. Chacón, and P. Tarazona, *Phys. Rev. E* **70**, 061601 (2004); P. Tarazona and E. Chacón, *Phys. Rev. B* **70**, 235407 (2004).
- <sup>10</sup>E. Velasco, P. Tarazona, M. Reinaldo-Falagán, and E. Chacón, *J. Chem. Phys.* **117**, 10777 (2002).
- <sup>11</sup>D. Li and S. A. Rice, *J. Phys. Chem.* **108**, 19640 (2004).
- <sup>12</sup>H. Mo, G. Evmenenko, S. Kewalramani, K. Kim, S. N. Ehrlich, and P. Dutta, *Phys. Rev. Lett.* **96**, 096107 (2006).
- <sup>13</sup>B. M. Ocko, X. Z. Wu, E. B. Sirota, S. K. Sinha, and M. Deutsch, *Phys. Rev. Lett.* **72**, 242 (1994).
- <sup>14</sup>M. K. Sanyal, S. K. Sinha, K. G. Huang and B. M. Ocko, *Phys. Rev. Lett.* **66**, 628 (1991).
- <sup>15</sup>W. Zhao, X. Zhao, J. Sokolov, M. H. Rafailovich, M. K. Sanyal, S. K. Sinha, B. H. Cao, M. W. Kim, and B. B. Sauer, *J. Chem. Phys.* **97**, 8536 (1992).
- <sup>16</sup>W. Zhao, M. H. Rafailovich, J. Sokolov, L. J. Fetters, R. Plano, M. K. Sanyal, S. K. Sinha, and B. B. Sauer, *Phys. Rev. Lett.* **70**, 1453 (1993).
- <sup>17</sup>A. Braslau, M. Deutsch, P. S. Pershan, A. H. Weiss, J. Als-Nielsen, and J. Bohr, *Phys. Rev. Lett.* **54**, 114 (1985).
- <sup>18</sup>O. Shpyrko, M. Fukuto, P. Pershan, B. Ocko, I. Kuzmenko, T. Gog, and M. Deutsch, *Phys. Rev. B* **69**, 245423 (2004).
- <sup>19</sup>B. M. Ocko, A. Braslau, P. S. Pershan, J. Als-Nielsen, and M. Deutsch, *Phys. Rev. Lett.* **57**, 94 (1986).
- <sup>20</sup>J. Als-Nielsen, F. Christensen, and P. S. Pershan, *Phys. Rev. Lett.* **48**, 1107 (1982).
- <sup>21</sup>J. M. Soler, G. Fabricus, and E. Artacho, *Surf. Sci.* **482**, 1314 (2001).
- <sup>22</sup>E. DiMasi, H. Tostmann, B. M. Ocko, P. S. Pershan, and M. Deutsch, *Phys. Rev. B* **58**, R13419 (1998).
- <sup>23</sup>M. J. Regan, P. S. Pershan, O. M. Magnussen, B. M. Ocko, M. Deutsch, and L. E. Berman, *Phys. Rev. B* **54**, 9730 (1996).
- <sup>24</sup>A. D. Abbott, J. R. Wright, A. Goldschmidt, W. T. Stewart, and R. O. Bolt, *J. Chem. Eng. Data* **6**, 437 (1961).
- <sup>25</sup>K. M. Klinecicz and R. C. Reid, *AIChE J.* **30**, 137 (1984).
- <sup>26</sup>C. J. Yu, A. G. Richter, J. Kmetko, S. W. Dugan, A. Datta, and P. Dutta, *Phys. Rev. E* **63**, 021205 (2001).
- <sup>27</sup>C. J. Yu, A. G. Richter, A. Datta, M. K. Durbin, and P. Dutta, *Phys. Rev. Lett.* **82**, 2326 (1999).
- <sup>28</sup>J. Maroto, F. J. de las Nieves, and M. Quesada-Perez, *Eur. J. Phys.* **25**, 297 (2004).
- <sup>29</sup>F. P. Buff, R. A. Lovett, and F. H. Stillinger, *Phys. Rev. Lett.* **15**, 621 (1965).
- <sup>30</sup>F. Celestini, F. Ercolessi, and E. Tosatti, *Phys. Rev. Lett.* **78**, 3153 (1997).
- <sup>31</sup>S. Iarlori, P. Carnevali, F. Celestini, F. Ercolessi, and E. Tosatti, *Surf. Sci.* **211**, 55 (1989).
- <sup>32</sup>I. M. Tidswell, B. M. Ocko, P. S. Pershan, S. R. Wasserman, G. M. Whitesides, and J. D. Axe, *Phys. Rev. B* **41**, 1111 (1990).
- <sup>33</sup>M. K. Sanyal, J. K. Basu, A. Datta, and S. Banerjee, *Europhys. Lett.* **36**, 265 (1996).
- <sup>34</sup>S. K. Sinha, *Curr. Opin. Solid State Mater. Sci.* **1**, 645 (1996).
- <sup>35</sup>See, e.g., X. Z. Wu, E. B. Sirota, S. K. Sinha, B. M. Ocko, and M. Deutsch, *Phys. Rev. Lett.* **70**, 958 (1993); X. Z. Wu *et al.*, *Science* **261**, 1018 (1993).